11

Experimental EMF Exposure Assessment

Sven Kühn and Niels Kuster

CONTENTS

11.1 Objectives and Limitations 381
11.1.1 Dosimetry 382
11.1.2 Densitometry or Incident Exposure Assessment 383
11.2 Fundamental Quantities of EMF 384
11.2.1 Primary Quantities: Basic Restrictions 385
11.2.2 Derived Quantities: Reference Levels or Maximum Permissible Exposure 386
11.3 Experimental Techniques 386
11.3.1 Field Probes 386
11.3.1.1 Broadband *E* Field Probes 386
11.3.1.2 Electro-Optical Sensors 389
11.3.2 Temperature Instrumentations 391
11.3.2.1 Temperature Probes 391
11.3.2.2 Infrared Photography 392
11.3.2.3 Microcapsulated Thermo-Chromic Liquid Crystals 393
11.3.2.4 Calorimeters 393
11.3.3 Measurement Antennas 393
11.4 Near-Field Scanners 394
11.4.1 Scanners for Dosimetric Compliance Testing 394
11.4.2 Fast Dosimetric Scanners 395
11.4.3 Incident Near-Field Scanners 397
11.5 Incident Field Evaluations in the Far Field of Transmitters 398
11.5.1 Broadband Measurements 399
11.5.2 Frequency-Selective Measurements 401
11.5.3 Code-Selective Measurements 402
11.6 Typical Maximum Peak Spatial SAR Exposures 402
11.7 Typical Far-Field Exposures 404
Acknowledgment 405
References 405

11.1 Objectives and Limitations

Experimental electromagnetic field (EMF) exposure assessments can be divided into two categories: (1) densitometry, that is, quantification of the incident EMF or the field characteristics at the location of exposed bodies but without their presence, and (2) dosimetry, that is, quantification of the EMF induced in biological tissues or bodies. In most cases of compliance evaluation, verification that the actual exposure is below a certain value is paramount to accurate determination of the individual exposure. However, highly accurate predictions are needed for some medical applications, for instance, hyperthermia. The focus of this chapter is on dosimetry for frequencies above 10 MHz, often referred to as radio frequency (RF) dosimetry. At lower frequencies, experimental dosimetry is usually limited to measurement of the incident magnetic fields.

11.1.1 Dosimetry

Dosimetry is the science of quantifying the three-dimensional (3–D) distribution of EMF inside tissues and organs of biological bodies. The term is also applied with media having dielectric characteristics similar to biological bodies, for example, cell cultures, tissue-simulating liquids, etc. The induced field is the only field parameter that can interact with biological processes and therefore is referred to as the primary quantity.

Dosimetry usually refers to the assessment of the induced fields on a macro level, that is, the averaged induced fields across cells. Microdosimetry refers to the evaluation of fields across membranes, proteins, etc. This is a new field facing various basic problems such as material models and transitions between classical and quantum electrodynamics. Since the field of microdosimetry has not yet matured and since microdosimetry can be directly developed from locally averaged induced fields in the frequency range considered (<300 MHz), the term dosimetry in this chapter refers to marcodosimetry only.

The distribution of induced fields, particularly at RF, is a complex function of numerous parameters such as frequency, incident field strength, incident angle, field impedance, incident field distribution, polarization, size and shape (posture) of the biological body, tissue distribution, dielectric characteristics of the tissues, etc. In general, the dynamics of the induced field strength range over several orders of magnitude. In other words, the strength and distributions of the fields induced by the same incident exposure greatly vary with anatomy and body orientation with respect to the field and posture.

It is practically impossible to measure the fields noninvasively or *in vivo*; thus, measurements can only be obtained postmortem. The limitations [1] associated with postmortem evaluations include (1) accessibility to only certain tissues, (2) dielectric changes (e.g., lower tissue temperature and decreased blood content), (3) field distortions by the invasively introduced probe, and (4) large uncertainties associated with obtaining accurate measurements near and across tissue boundaries [2,3]. Only the integrated, totally absorbed power can be determined relatively easily by the calorimeter method (see Section 11.3.2.4).

Progress in computational electromagnetics along with the exponential growth of computational power and memory have facilitated determination of the field distributions in full anatomical human bodies with resolutions much smaller than 1 mm^3 (see Chapter 10 on RF modeling by Lin). The lossy and low-resonance properties of complex anatomical structures pose no special challenges for numerical methods (Figure 11.1). Limitations are only due to inadequate phantoms providing insufficient spatial resolution, for example, to accurately represent the scull [3].

Nevertheless, experimental dosimetry is often superior to numerical approaches for the compliance testing of commercial devices. Sources usually consist of highly resonant structures tightly assembled with other electronic and metallic structures. It is difficult to predict with reasonable and known uncertainty whether and how distortion of resonances and excitations of secondary structures might occur through simulations, especially when also considering the scattered fields of biological bodies. Small differences can

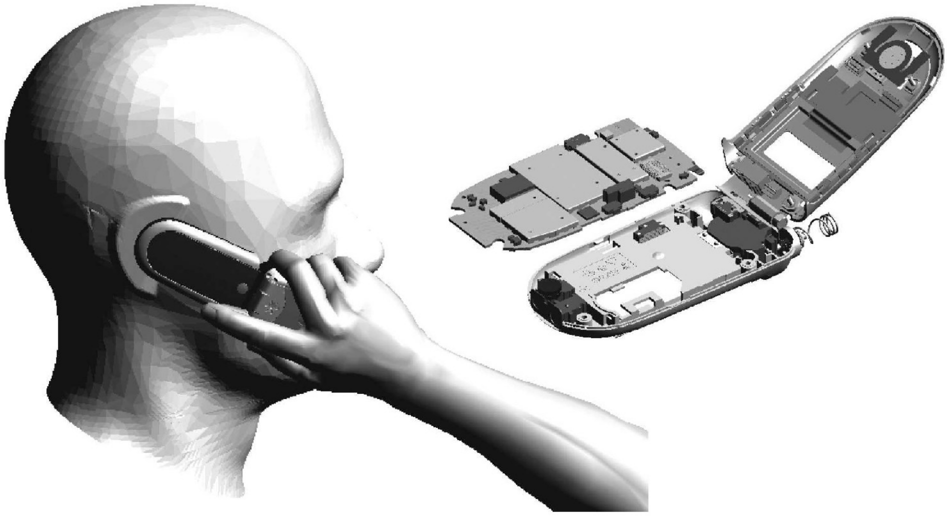

FIGURE 11.1
The latest advances in numerical techniques enable the computation of realistic scenarios without restrictions regarding spatial resolution and material description. The remaining difficulties are material parameters and manufacturing tolerances.

easily result in deviations of more than a factor of 2 from reality. Only when the structure is electromagnetically well-defined can good correspondence between simulations and measurement generally be achieved, that is, with an uncertainty smaller than 20% [4]. On the other hand, experimental techniques allow testing of the physical device under test (DUT) and do not require verification of the computational model.

The detailed information of the field distributions inside anatomical bodies obtainable by numerical methods is often irrelevant, since it cannot be generalized. For safety considerations, the upper boundary of exposure for the entire population rather than individual exposure is relevant. Hence, worst-case phantoms are often applied to assess the upper exposure boundary for specific exposure conditions, for example, from mobile transmitters. Since the degree of freedom for these phantoms is relatively large, they can be chosen homogenously (see Section 11.4.1). Recent evaluation of the procedures for mobile phone compliance testing has confirmed that conservative assessments are possible with a simplified experimental technique using homogenous phantoms [4–6].

During the past decade, considerable progress has been achieved in experimental dosimetric assessment. Since the late 1990s, experimental techniques have been routinely applied for evaluating transmitters operating in the closest vicinity of the body. They have proven to be more reliable, cheaper, and faster. A summary of these techniques and procedures is provided in this chapter. However, dosimetric assessments are limited to homogenous phantoms or to a few tissues in biological bodies. These assessments are normally applied for testing compliance with the basic restrictions or for the validation of results obtained by computational techniques.

11.1.2 Densitometry or Incident Exposure Assessment

Experimental dosimetry requires sophisticated instrumentation, significant expertise, and time. It is impractical for *in situ* exposure assessments. Therefore, easy to apply techniques and methods using a worst-case approach have been developed to determine compliance with potentially hazardous induced fields by determining the incident fields. The worst-case concept derives the conditions for maximum induced fields inside the human body for an incident field strength in terms of the polarization, field distribution (plane wave), field impedance (plane wave), size, and posture of the human body and its dielectric properties. The induced fields are lower than a value X if the local maximum incident field strength of the E field and H field is below the value Y. Attempts to alter this conservative approach have yielded alternatives with an insufficient scientific and engineering basis (see Section 11.5).

Assessment of the incident exposure is simple for plane wave or far-field conditions. Under these conditions, the E field vector is perpendicular to the H field vector, and both are orthogonal to the direction of propagation. The ratio of the E and H fields is equal to the wave impedance Z at any location:

$$Z = \frac{E}{H} \tag{11.1}$$

and in free space

$$Z_0 = 377\,\Omega \tag{11.2}$$

Furthermore, the amplitude is constant over the entire volume of the absent exposed body. In these cases, it is necessary to measure only one component (E or H field) at one location in space. Unfortunately, far-field conditions rarely occur. However, far-field conditions are approximately met locally by changing the amplitude in space at distances larger than the extension of the reactive near-field zone:

$$r > \frac{2D^2}{\lambda}, \quad D \sim \frac{\lambda}{2} \tag{11.3}$$

$$r > \frac{\lambda}{2\pi}, \quad D \ll \frac{\lambda}{2} \tag{11.4}$$

where r is the radius or distance from the transmitting antenna/structure, λ the wavelength, and D the largest antenna dimension.

In other words, for distances meeting the requirements of Equation 11.3 and Equation 11.4, only the maximum of the field components must be determined to demonstrate compliance.

For any distance smaller than the requirements of Equation 11.3 and Equation 11.4, the maximum of both components must be spatially scanned to reliably predict that the maximal induced fields are below a certain limit. Fine volume scanning of transmitter antennas in the very near field yields greater uncertainty and is more time-consuming than dosimetric measurement in homogenous phantoms. Since such near-field assessments are more conservative than specific absorption rate (SAR) evaluations, they are rarely conducted in the context of exposure assessments.

11.2 Fundamental Quantities of EMF

The basic quantities necessary for electromagnetic exposure assessment are summarized in Table 11.1.

TABLE 11.1

Quantities, Symbols, and Units Used in Experimental Exposure Assessment

Symbol	Quantity	Unit
$\vec{E}$	E field (vector)	V/m
$\vec{H}$	E field (vector)	A/m
S	Power density (scalar)	W/m^2
$\vec{S}$	Pointing vector, $\vec{S} = \vec{E} \times \vec{H}$	W/m^2
W	Energy density	W/m^3
SAR	Specific absorption rate	W/kg
ΔT	Temperature increase	K
J	Current density	A/m^2
$\bar{\varepsilon}$	Complex permittivity, $\bar{\varepsilon} = \varepsilon_0 \cdot \bar{\varepsilon}_r$	F/m
ε_0	Permittivity of free space, $\varepsilon_0 = 8.854 \times 10^{-12}$	F/m
$\overline{\varepsilon_r}$	Complex relative permittivity, $\overline{\varepsilon_r} = \varepsilon_r' - j\varepsilon_r''$	
σ	Conductivity	S/m
μ	Permeability, $\mu = \mu_r \cdot \mu_0$	H/m
μ_0	Permeability of free space, $\mu_0 = 4\pi \times 10^{-7}$	H/m
μ_r	Relative permeability	
c	Specific heat capacity	J/(kg K)
ρ	Mass density	kg/m^3

11.2.1 Primary Quantities: Basic Restrictions

Restrictions on exposure to time-varying electric fields, magnetic fields, and EMF that are based directly on established health effects are termed basic restrictions (see Chapter 8 on standards by Van Deventer et al. [68]). Depending on the frequency of the field, the physical quantities used to specify these restrictions are either the current density (J) or the SAR. The dosimetric quantities used in current guidelines [7–10] are J for frequencies up to 10 MHz and the SAR for the frequency range from 100 kHz to 10 GHz. J is related to the internal electric field by Ohm's law:

$$J = \sigma E \tag{11.5}$$

E is the internal electric field, and σ is the complex conductivity of the tissue.

SAR is the ratio of the average rate of the absorbed power to the absorbing mass. It is defined as follows:

$$\mathrm{SAR} = \frac{\mathrm{d}}{\mathrm{d}t}\left(\frac{\mathrm{d}W}{\mathrm{d}m}\right) = \frac{\mathrm{d}}{\mathrm{d}t}\left(\frac{\mathrm{d}W}{\rho \mathrm{d}V}\right) \tag{11.6}$$

where dW is the incremental energy dissipated in an incremental mass dm included in an incremental volume dV and ρ is the mass density. SAR can also be calculated directly from the electrical loss, which is proportional to the mean square of the locally induced electric field strength E:

$$\mathrm{SAR} = \frac{\sigma E^2}{\rho} = \frac{J^2}{\sigma \rho} \tag{11.7}$$

and to a temperature increase by:

$$\mathrm{SAR} = c\frac{\mathrm{d}T}{\mathrm{d}t} \tag{11.8}$$

where c is the local specific heat capacity of the tissue. Equation 11.8 is valid only if the exposed body is in thermal equilibrium or in a steady thermal state at the beginning of the exposure, and either heat exchange processes can be neglected during the measurement interval or the processes are known to correct dT correspondingly. Current safety standards [7–10] for limiting EMF exposure provide maximum limits for basic restrictions for the uncontrolled/general public as well as for controlled/occupational exposure over the whole considered frequency range. The standards are ambivalent with respect to the quantity SAR. The debate among experts is whether SAR is a dosimetric quantity only relevant as a surrogate for thermally based models of EMF interaction or whether it can describe effects in addition to those related to temperature. SAR is directly related to the induced internal E fields as well as to the current density (Equation 11.7) but only directly related to the induced H fields for special cases.

11.2.2 Derived Quantities: Reference Levels or Maximum Permissible Exposure

The derived quantities are the electric field strength (E), magnetic field strength (H), magnetic flux density (B), and power density (S). As discussed in the previous sections, these quantities were derived from the basic restrictions using experimental or computational methods and represent conservative limits for worst-case exposure scenarios. Derived limits are called reference [7] or maximum permissible exposure levels [8,9]. Compliance with these quantities implies compliance with the basic restrictions. However, if the reference quantities exceed the derived limits, the relevant basic restrictions are not necessarily exceeded. In such cases, compliance can be demonstrated by dosimetric means.

In summary, reference levels are easy to assess if the plane wave or far-field conditions are met (see Section 11.1.2) and the resulting SAR and induced current densities are below the corresponding basic restrictions under all circumstances. Typical reference limits for occupational/controlled and general public/uncontrolled exposure are given in Refs. [7–10].

11.3 Experimental Techniques

11.3.1 Field Probes

E field probes have been used for microwave measurement since the early 1970s. The first power meters were developed by Aslan [11] and Rudge [12]. Aslan used a thermocoupling model consisting of two pairs of thin-film, vacuum-evaporated electrothermic elements that functioned as both an antenna and a detector. Rudge employed two small diode-loaded dipoles as sensor elements. The first prototype of an isotropic, miniature field probe was introduced by Bassen et al. [13] in 1975. Additionally, fiber optic field probes had already been proposed in the 1970s [14]. Comprehensive overviews of field probes are reported in Refs. [2,15].

11.3.1.1 Broadband E *Field Probes*

Diode-based field probes are well established and commonly used for dosimetric assessment. These probes consist of an appropriate field sensor, a detector, transmission lines, and read-out electronics (Figure 11.2). Three mutually orthogonal diode-loaded dipoles with an isotropic receiving pattern constitute the probe. To achieve good spatial resolution and broadband performance, electrically short dipoles are employed:

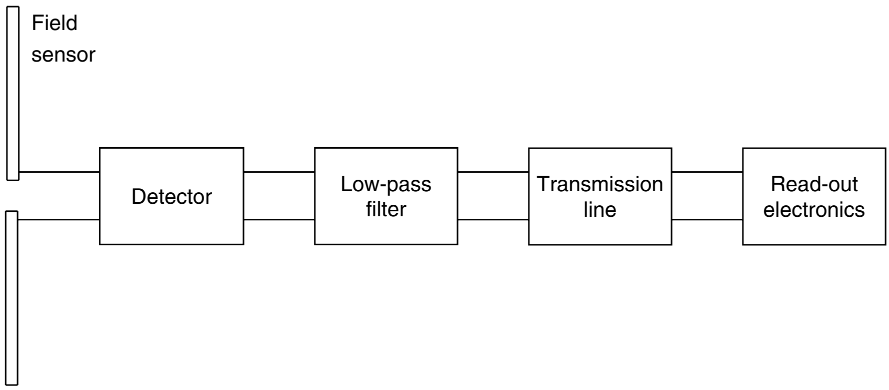

FIGURE 11.2
Simplified schematic of a broadband field probe.

$$\beta h = \frac{2\pi h}{\lambda} \ll 1 \tag{11.9}$$

where h is the length of a dipole arm, β the propagation constant, and λ the wavelength [15]. A flat frequency dependence cannot be achieved if the length of the probe is larger than a fraction of the wavelength ($< 0.05\lambda$). However, this limitation can be overcome by gradually resistive dipoles [16].

Typical isotropic E field probe sensors are shown in Figure 11.3. An RF detector diode (usually Schottky type) is located in the center of the dipole arms. If the detector diode is operated in the square-root law region, the diode current is proportional to the RF power delivered over the dipole to the detector diode. The detector diode is connected with a highly resistive line to the data acquisition electronics. The transmission lines must be designed precisely to eliminate distortions, such as parasitic sensor elements and scattering, which cause degradation of the pattern and unwanted polarization characteristics of the actual receiving antenna. High-resistive transmission lines are ideal for minimizing field perturbation and pickup effects. A detailed investigation of transmission line design

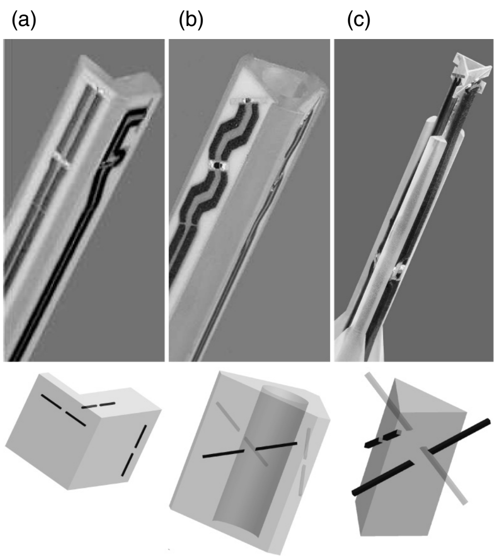

FIGURE 11.3
E field probe configurations: (a) E field probe for measurements in air with one sensor aligned to the probe axis and two orthogonally, (b) dosimetric probe for E field measurements in tissue-simulating liquids allowing integration of an optical proximity sensor in its center, and (c) miniature dosimetric probe with interleaved dipoles. (From IT'IS Foundation. With permission.)

can be found in Smith [17]. Current probe designs apply either thin-film ($R \sim 10$ MΩ/m) [14] or thick-film ($R \sim 500$ MΩ/m) [18] techniques.

The induced fields are recorded by the read-out electronics. The electronics typically consist of a measurement amplifier and an analog digital converter. The read-out field values are then optically forwarded. The optical transmission provides a galvanic decoupling and reduction of field-perturbing conductive parts near the DUT.

In addition to *E* field probes, *H* field probes are also available, the basic theory of which can be found in Whiteside and King [19]. *H* field probes and *E* field probes are basically similar, except for the field sensor element, that is, *H* field probes employ a small loop element instead of a dipole sensor. The disadvantages of loop-based sensors include a strong frequency dependence and currents induced by both *H* and *E* fields. Different methods for flattening the frequency dependence of loop probes have been proposed in Refs. [2,20]. The ratio of the voltage induced in a circular loop with diameter *d* by the *E* field and the *H* field is [19]:

$$\frac{V_E}{V_H} \simeq -j2\pi \frac{d}{\pi} \tag{11.10}$$

Therefore, for electrically small loops only, that is, $d/\lambda \ll 0.01$, the current will mainly be determined by the magnetic field. In Poković [2], lossy covers were proposed to suppress the *E* field sensitivity of the loop.

In contrast to dipole-based sensors, thermocouple probes are true square-root law [a1]detectors. Such sensors are, for example, used in free space field probes by Narda [21]. These sensors are, however, impractical for dosimetric and near-field applications because of their generally lower sensitivity and dynamic range.

Thermistors are also true square-root law detectors and also small. They can have higher resolution than thermocouples but need more frequent calibration.

Based on the setup of these isotropic field probes, the measured field magnitude is yielded from the root sum square of the three orthogonal components:

$$|X| = \sqrt{|X_1|^2 + |X_2|^2 + |X_3|^2}\; X \in \{E,H\} \tag{11.11}$$

This summation is carried out regardless of any phase differences between the respective components. Hence, if maximum hold peak detectors are applied, the field reading represents the upper bound of the field magnitude.

The output signal of the probes just described is dependent on the following parameters:

- Frequency, modulation, and field strength
- Polarization, direction, and field gradients
- Material boundaries near the probe sensors
- Sources of interference (noise, static and low-frequency fields, vibration, temperature, etc.).

Therefore, it is necessary to quantify the influence of these parameters. Calibration under well-defined conditions is carried out to characterize the most crucial parameters for each probe individually. A detailed summary of different calibration methods for field probes and characterization of the parameters contributing to the measurement uncertainty is given in Poković [2]. All possible influences must be included in the resulting uncertainty assessment, since the conditions during the actual application of the probes differ

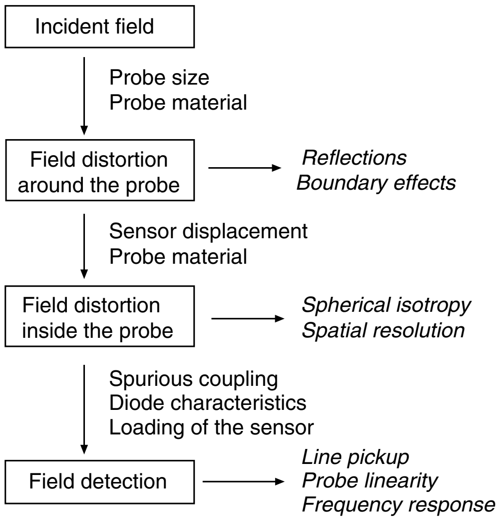

FIGURE 11.4
Impact of the constructional details on the probe characteristics.

considerably from the calibration scenario. Figure 11.4 provides an overview of different probe construction parameters that contribute to the probe characteristics.

Modern dosimetric field probes are available in the frequency range from 10 MHz up to 6 GHz. They have an isotropy error lower than ± 0.5 dB and sensitivities in the range of 1–10 μW/g [22]. Modern probes have very small sensor tip dimensions (2.5 mm) and high spatial resolution, allowing measurements very close to material boundaries. A probe with reduced size (tip diameter 1.0 mm) was introduced by Poković et al. [23] and enables accurate dosimetric measurements for frequencies exceeding 10 GHz. Although this probe consists of only a single sensor element, isotropy is obtained by 120° rotation around the probe axis and an appropriately aligned sensor element. Probes for determining both the electrical and the magnetic field vector information are presented by Poković et al. [24]. This technique is based on measurements of five or more field components in space and reconstruction of the ellipse parameters by a combination of a downhill simplex and a Givens updating algorithm.

11.3.1.2 Electro-Optical Sensors

In contrast to RMS sensors, it is possible to measure fields over a broad frequency band in the time domain by exploiting electro-optic methods. Recent advances in semiconductor and photonic crystal research have provided the foundation for the next generation of near-field measurement equipment based on electro-optical methods. The basic concept of electro-optic probes is shown in Figure 11.5.

The most important electro-optic effects for measuring EMF are the Pockels effect and the quantum confined Stark effect (QCSE). The Pockels effect describes the refraction index dependence on the induced E field of anisotropic dielectric crystals such as cadmium telluride (CdTe) [25] or lithium nobiat ($LiNbO_3$) [26,27]. H field-sensitive crystals have also been determined, for example, cadmium manganese telluride (CdMnTe) [25]. The QCSE is based on the change of the absorption spectrum of a semiconductor structure under the influence of the electric field. Sensors exploiting the Pockels effect are reported in Refs. [25–27]. A detailed summary of electro-optic phenomena, materials, and applications can be found in Agullo-Lopez et al. [28]. Alternatively, the signal from the field sensor can modulate a small laser diode rather than the external electro-optical modulation.

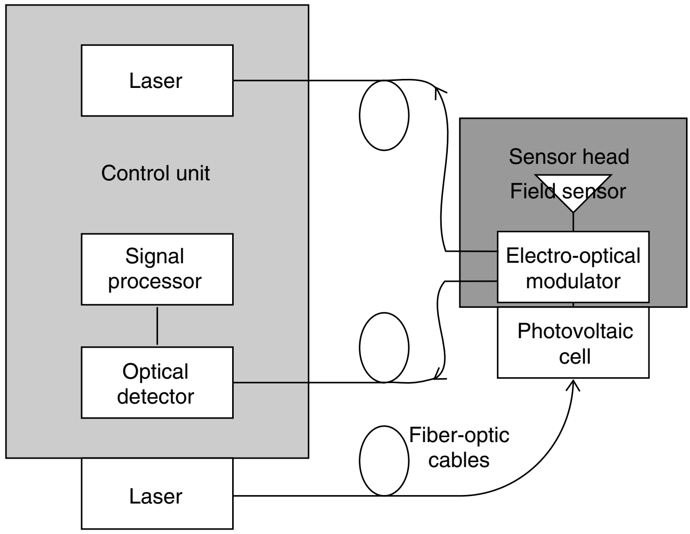

FIGURE 11.5
Principle of an electro-optic probe for EMF measurements.

The most common modulators are the Mach–Zehnder interferometer (MZI) as well as the already mentioned method of the direct modulation of the laser-diode current. The MZI (Figure 11.6) splits the light of a single-mode fiber into two parallel branches of $LiNbO_3$ waveguides. The feedpoints of the dipole are connected to electrodes that are located between the parallel branches, resulting in the antipodal modulation of the phase of the light. For recombined light, the phase modulation results in an intensity modulation. Sensitivities of 1–10 mV/(m Hz) can be reached. The upper cutoff frequency of these sensors is primarily determined by the length of the branches. For high sensitivity, the transit time through the interferometer must be much lower than the periodic time of the signal being measured. In Refs. [26,27], interferometers with a 3-dB bandwidth of 10 GHz were realized. A possibility to overcome this limitation could be the application of traveling wave modulation [29].

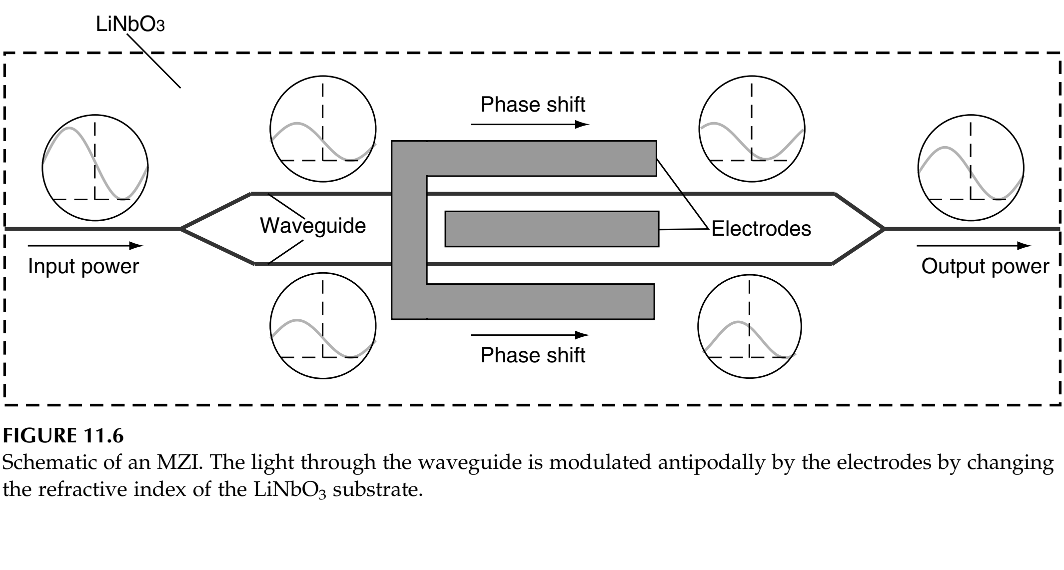

FIGURE 11.6
Schematic of an MZI. The light through the waveguide is modulated antipodally by the electrodes by changing the refractive index of the $LiNbO_3$ substrate.

Another approach reported in Ref. [25] uses only nonconductive parts in the sensor tip. Different types of crystals that are sensitive to electric and magnetic fields are used. Linear polarized light passing through the electro-optic crystal is reflected on a dielectric mirror and passes through the crystal again, where the polarization is changed. A beam-split polarizer transduces the ellipticity change into a change of the optical intensity. Sensors with a sensitivity of 10–400 V/m and 0.1–0.8 A/m in the frequency range from DC to 2 GHz were realized.

For modulation using QCSE, semiconductors with pn- or pin-junction structures are used. A varying reverse bias over the junction modulates the electric field and consequently the absorption and reflection spectra of the semiconductor as well. If the modulator is operated at a constant frequency, different reflection and transmission characteristics of the light and an intensity modulation result.

In addition to passive modulation (QCSE), direct modulation of a vertical cavity surface emitting laser (VCSEL) [30–32] has recently been applied. The current through the laser is directly modulated by the measurement signal. The VCSEL is especially suitable for modulation because of its high bandwidth, low threshold current, and low noise.

The MZI is the most popular modulation method among the three mentioned, and several commercial products are available based on this technology. Disadvantages include the limited ability to reduce its size as well as the bandwidth limitations. Passive modulators are relatively simple to manufacture as integrated circuits. Although passive modulators are inferior to MZI regarding sensitivity, the development of miniature field probes applying the VSCEL technology is currently the most promising approach.

11.3.2 Temperature Instrumentations

11.3.2.1 Temperature Probes

The locally induced SAR can also be assessed by temperature measurements, as summarized in Equation 11.8. A typical temperature rise curve as applied for SAR measurements is shown in Figure 11.7. Two types of temperature probes exist: those based on thermistors and those based on optical effects. The requirements for temperature probes for SAR assessments are:

- *Small size:* The probe must be small to resolve high temperature gradients, without disturbing the temperature distribution as well as the RF field.
- *Nonconductive materials:* Only electrically nonconductive materials prevent heating of the probe by induced currents and are transparent to EMF.
- *Low noise level:* Especially for dynamic temperature measurements, for example, SAR, small differences must be detected accurately. Therefore, the noise level should be much smaller than 10 mK.
- *Short reaction time:* A short reaction time is essential for SAR measurements, since the temperature rise ($\mathrm{d}T/\mathrm{d}t$) is only proportional to the SAR if heat diffusion does not occur. An appropriate probe must have reaction times much lower than 100 msec [33].

Temperature probes for SAR measurement using thermistors were first described by Bowman [34]. These probes utilize high-resistance thermistors that are connected through high-resistance lines to the read-out electronics. In Burkhardt et al. [35], a temperature probe based on a VITEK thermistor (BSD Medical Devices, U.S.A.) is presented. This probe has a noise level of 5 mK, a sensitivity of 5 mK/sec, and a tip diameter of

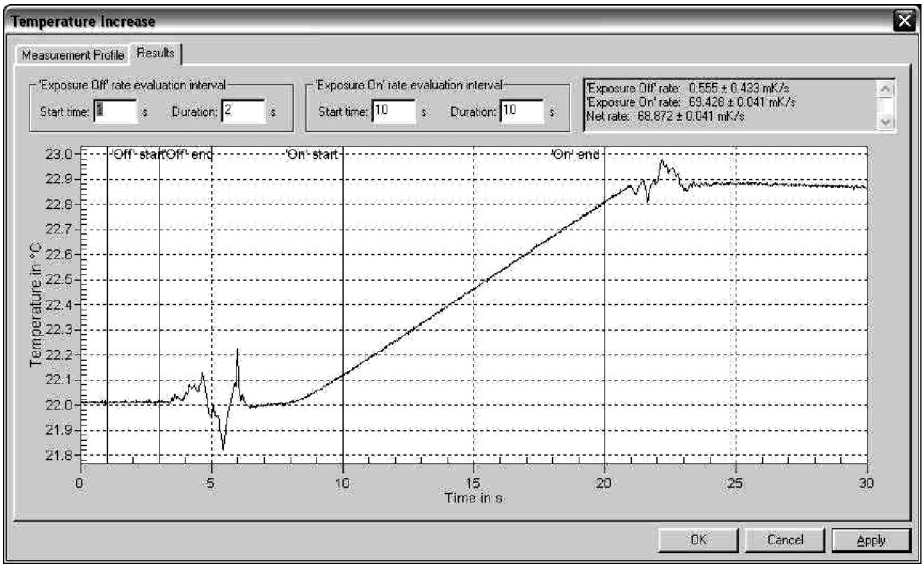

FIGURE 11.7
Typical temperature rise curve for SAR assessment. The linear part of the rise curve is applied for the calculation of the SAR. (Acquired using DASY4 from SPEAG, Switzerland.)

1 mm; however, it has a relatively slow response time of 240 msec. In Schuderer et al. [36], a novel temperature probe design for dosimetric assessments was introduced. The probe provides a spatial resolution of 0.02 mm^3, noise level of 4 mK, a sensitivity of 0.5 mK/sec, as well as a response time of only 10 msec.

In addition to the thermistor concept, temperature probes based on thermo-optical effects are also available. These probes are applied in high-voltage transformers, industrial microwave ovens, and hyperthermia treatment. One of the exploited effects is the decay rate of a phosphorescent layer at the tip of a fiber optic cable [37]. These modern commercially available probes have a noise level of 0.1 K and reaction times of 250 msec. Another exploited effect is the interferometric application of a cavity that is filled with materials that have highly temperature-dependent refraction indices. These probes reach sensitivities of 2–3 mK/sec [35].

11.3.2.2 Infrared Photography

The measurement of temperature by black body-equivalent radiation (infrared photography) is an alternative to invasive measurements using temperature probes. The resolution of infrared thermographs can be very high (<1 mm), and the sensitivity of affordable systems has continuously improved over the years. This was also one of the first methods to measure SAR [38], since the surface radiation can be recorded quickly using infrared cameras without perturbation of the incident field. Infrared cameras were also used to measure the temperature of Global System for Mobile Communications (GSM) mobile phones [39]. The technique has several disadvantages:

- It has limited sensitivity compared to temperature or dosimetric probes.
- It is limited to surfaces.

- The thermal radiation characteristics of the materials must be determined accurately.
- The background radiation must be homogenous.
- Evaporation and convection can cause substantial errors and must be controlled.
- Different aspect angles of the camera can cause different results.

11.3.2.3 Microcapsulated Thermo-Chromic Liquid Crystals

A novel idea to assess 3-D temperature distributions optically and in quasi real time was proposed by Suzuki et al. [40]. Microcapsulated thermo-chromic liquid crystals are suspended uniformly in a gel with the dielectric properties of human muscle tissue. The temperature of the gel is determined by measuring the light scattered from a laser beam that scans through the liquid. The technique has a limited dynamic range and sensitivity.

11.3.2.4 Calorimeters

Calorimetry specifies methods for measuring heat due to biological, chemical, or physical processes that are endothermic or exothermic. Calorimetric methods are suitable for determining average whole-body SAR, but they cannot reveal SAR distributions.

Calorimetry can be subdivided into two types:

- *Direct calorimetry:* The heat is determined directly using calorimeters.
- *Indirect calorimetry:* The amount of expressed heat is determined indirectly by measuring the amount of oxygen consumption and relating it to the oxicaloric equivalent of the reaction.

Basically, calorimetric dosimetry analyzes the heating and cooling processes of an exposed sample. Typical calorimeters used in microwave dosimetry are the Dewer flask calorimeter and the twin-well calorimeter [41].

11.3.3 Measurement Antennas

Different types of broadband matched antennas are usually applied for the frequency-selective exposure assessment of external fields. These measurement antennas are matched to 50 Ω to be compatible with standard RF measurement equipment. They are usually applied for far-field measurements of emissions by cellular telephony base stations, broadcast services, etc. Common broadband RF measurement antennas such as horn or logarithmic periodic antennas have a certain directivity. For example, for an antenna with a 45° beam width, more than 18 measurement directions are necessary for each polarization, since the receiving patterns do not have the shapes of square sectors. This reduces the applicability of these antennas for complex propagation scenarios, that is, locations where the received field is not dominated by a direct line of sight propagation path but by multipath reception. Tuned dipole antennas do not show a directivity in the radial direction, but they lack broadband operation. Conical [42] and biconical [43] antennas have the advantage of nondirectiveness in the radial direction and generally good broadband characteristics. If, for example, the ADD3D method [44] is applied in combination with a conical dipole antenna, the measurement orientations for a fully isotropic scan can be reduced to three different directions. In this case, the isotropy is obtained by an antenna alignment similar to near-field probes, such that the resulting field is:

$$|E| = \sqrt{|E_1|^2 + |E_2|^2 + |E_3|^2} = \sqrt{|U_1|^2 + |U_2|^2 + |U_3|^2} \cdot AF \tag{11.12}$$

where AF is the frequency-dependent antenna factor in linear quantities (1/m) and U_i is the antenna output voltage at the three different antenna orientations. To obtain the antenna output voltages, a measurement receiver (see Section 11.5.1) connected via a well-characterized cable is applied. The antenna output voltage is:

$$|U_{i_{\text{antenna}}}| = |U_{i_{\text{receiver}}}| \cdot \text{ATT}_{\text{cable}} \tag{11.13}$$

where $|U_{i_{\text{receiver}}}|$ is the voltage measured with the receiver and $\text{ATT}_{\text{cable}}$ the attenuation of the cable in linear units. Other sources of attenuation, for example, attenuators to reduce the Voltage standing wave ratio (VSWR) of the measurement antenna, must be similarly considered.

11.4 Near-Field Scanners

11.4.1 Scanners for Dosimetric Compliance Testing

In dosimetric compliance tests, exposures from RF transmitters operating in close proximity to the body, for example, mobile phones or body-worn wireless devices, are compared to the basic restrictions (see Section 11.2.1). This is a complex task, since the exposure greatly depends on the device design, the position of the device with respect to the body, the external and internal anatomy, as well as the effect of the backscattered field on the device (Figure 11.8). In order to obtain a reliable assessment with acceptable effort, the standards must determine the maximum or 90th percentile exposure for the entire

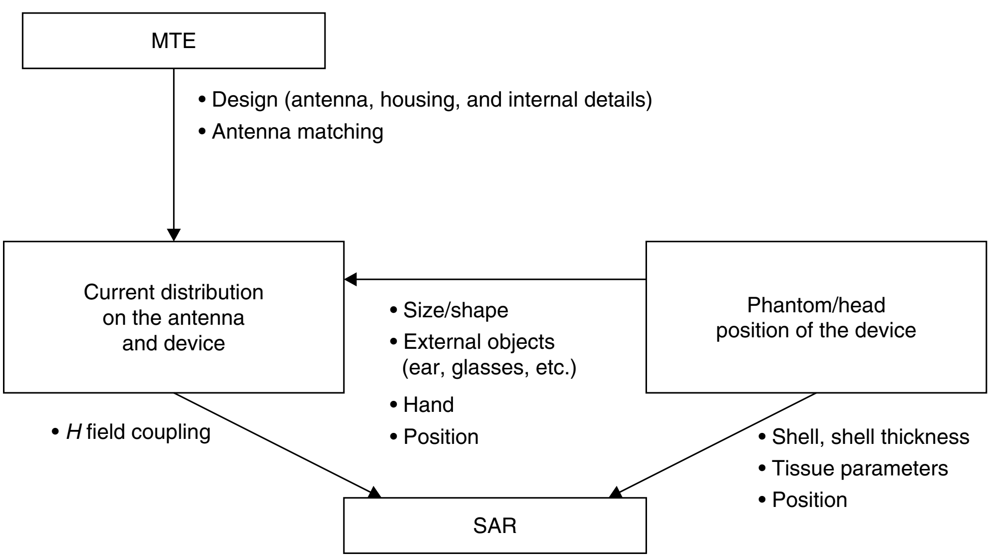

FIGURE 11.8
Overview of impact parameters for dosimetric compliance testing of mobile terminal equipment (MTE).

population that may be operating the DUT. Measurement standards have been developed by different organizations, for example, by the International Electrotechnical Commission (IEC), the Institute of Electrical and Electronics Engineers (IEEE), the Association of Radio Industries and Businesses (ARIB), Korea Electromagnetic Engineering Society (KEES), and others.

In general, a dosimetric evaluation requires the measurement of several hundreds of points distributed over a complex 3-D phantom. The task is divided into (1) searching for the location of the maximum absorption on a 2-D grid and (2) determining the peak spatial SAR value on a fine 3-D grid. Especially at high frequencies, these points must be determined with high accuracy to achieve low measurement uncertainty despite high attenuation and large spatial field variations. Automated dosimetric assessment systems are utilized to perform these compliance tests. A typical configuration of a dosimetric assessment system is shown in Figure 11.9 and Figure 11.10. A computer-controlled six-axis positioner with excellent positioning repeatability of ± 0.2 mm is used to move the dosimetric E field probe within the scanning grid, which can be adaptive, for example, along a surface that is being detected during the scanning job. The different field probe designs have already been discussed in Section 11.3.1. Phantoms, for example, the specific anthropomorphic mannequin (SAM) phantom, elliptical phantom, etc., and tissue-simulating liquids (see Table 11.2) have been developed and validated with respect to the 90th percentile requirements [45]. A detailed description is provided by Schmid et al. [18]. Because of the strong curvature of the SAM phantom, sufficient accuracy can be obtained only when the measurements are taken with the probes aligned normal to the phantom boundary. The most elaborated components, procedures, and algorithms are employed (Figure 11.10), and an expanded total uncertainty ($k = 2$) for the compliance test of less than 20% can be achieved with even better repeatability.

It should be noted that this approach provides reliable conservative estimates of the maximum peak spatial SAR that might occur in the user population but little information about the exposure of specific tissues.

11.4.2 Fast Dosimetric Scanners

Dosimetric compliance tests of near-field sources are extremely time-consuming, especially as all configurations with all accessories must be evaluated. SAR patterns provide

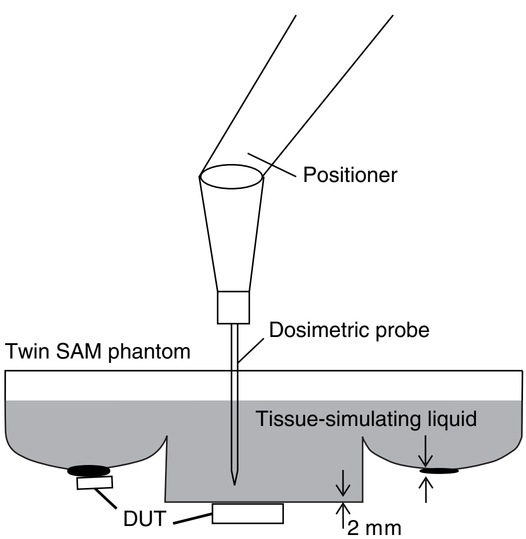

FIGURE 11.9
A dosimetric assessment systems consists of a computer-controlled positioner, a dosimetric field probe, and a phantom (left and right head, flat region for system validation) filled with tissue-simulating liquid.

FIGURE 11.10
DASY4 dosimetric assessment system. (From SPEAG, Switzerland.)

further valuable information such as (1) the output power under loaded conditions as indicated by a different peak spatial SAR if the absorption pattern is not altered and (2) changes in the internal RF path, for instance, by poor contacts, as indicated by a modified SAR pattern. Therefore, fast SAR scanners are desirable for precompliance testing as well as for research and development. Such scanners would also be greatly beneficial for

TABLE 11.2
Electric Parameters of Head and Body Tissue Equivalent Liquids at Various Frequencies

	Head		Body	
Frequency (MHz)	ε_r	σ (S/m)	ε_r	σ (S/m)
150	52.3	0.76	61.9	0.80
300	45.3	0.87	58.2	0.92
450	43.5	0.87	56.7	0.94
835	41.5	0.90	55.2	0.97
900	41.5	0.97	55.0	1.05
915	41.5	0.98	55.0	1.06
1450	40.5	1.20	54.0	1.30
1610	40.3	1.29	53.8	1.40
1800–2000	40.0	1.40	53.3	1.52
2450	39.2	1.80	52.7	1.95
3000	38.5	2.40	52.0	2.73
5800	35.3	5.27	48.2	6.00

quality assurance purposes, when integrated into production lines (every device tested for compliance, output power, and RF performance).

An algorithm to extrapolate peak spatial SAR values from the 2-D area scan performed at the phantom surface was presented by Kanda et al. [46]. Another algorithm reducing the measurement time of an area scan lasting 5–10 min was proposed by Merckel and Fleury [47].

Two additional approaches have been presented to further accelerate the assessment. The first approach, using a scanner based on incident *H* field measurements, is described in the next section. The second approach is based on a sensor array implanted in a solid flat phantom (Figure 11.11). The phantom is filled with a broadband tissue-simulating gel (300 MHz up to 6 GHz), with sensors located 4 mm below the surface. The density of the sensor array (15 mm) is sufficient to reliably assess the exposure. The measured SAR values of all sensors are acquired and integrated in parallel, such that the total assessment time is less than 3 sec, even for TDMA (Time Division Multiple Access) signals with complicated frame structures.

11.4.3 Incident Near-Field Scanners

In the reactive near field, field gradients are generally very high, and the field impedance differs greatly from the far-field impedance and rapidly changes over short distances. Hence, both *E* and *H* fields must be assessed, based on requirements regarding spatial resolution and isotropy that are similar to those of dosimetric scanners. In addition, distortions by reflections from instrumentation must also be carefully evaluated and included in the uncertainty budget.

General purpose scanner systems are equal or similar to those used for dosimetric evaluations, except that *E* and *H* field probes optimized for free space are used instead of

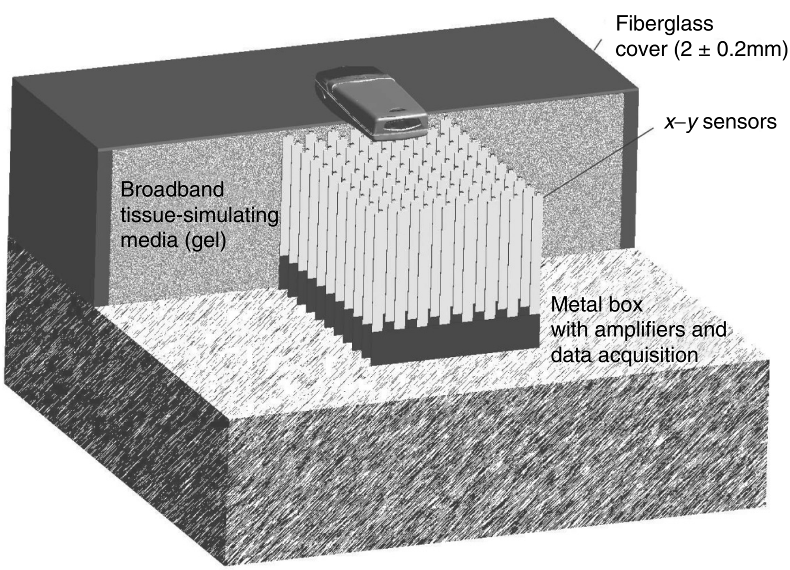

FIGURE 11.11
The concept of a fast dosimetric scanner based on a dense array of sensors completely immersed in a broadband tissue-simulating medium. In order to provide a quick response, the signals of all sensors must be amplified and integrated in parallel for the frame structure and to increase the signal-to-noise ratio. The high-resistive sensor leads are vertical to minimize field distortions.

dosimetric probes. Since the scan procedures do not need to follow complex surfaces, three-axis systems [48] are also suitable. However, such evaluations are rarely used to test compliance with safety limits, since the limits are significantly more conservative and the measurement resources, time required, and uncertainty budget are higher than for dosimetric assessments. Nevertheless, such measurements are valuable for the validation of numerical results [49] or to test compliance with interference limits in the close near field, for example, for hearing aids [50].

A specialized near-field scanner was proposed and developed to test the precompliance of mobile handsets with safety limits [51]. Its underlining concept is based on the primary interaction mechanism of near-field exposure [52], that is, the local SAR is approximately proportional to the square of the incident magnetic field at the surface of the phantom:

$$\mathrm{SAR} = \alpha H_{\mathrm{s}}^{2} \tag{11.14}$$

The magnetic field is scanned in a reference plane above the DUT using a loop antenna array. The factor α is determined by relating a traditional compliance measurement inside the phantom to the magnetic field scan in free space for a certain DUT. The system can predict the SAR within 30 sec. The main disadvantage of such a system is that it does not simulate a realistic load to the antenna of the DUT.

11.5 Incident Field Evaluations in the Far Field of Transmitters

Evaluation of the exposure in the far field of a transmitter is usually conducted for fixed transmitters such as radio and TV broadcast antennas, radar sites, or cellular base stations. Exposure assessments are carried out in areas that are generally accessible or restricted to qualified working personnel. Compliance is tested with the reference limits by assuming free space field impedance, that is, by *E* field evaluation. As described in Section 11.1.2, only one measurement point is required under real far-field conditions. However, actual environments usually involve nearby reflectors, that is, a scanning procedure or statistical knowledge about the field distribution is needed to determine the maximum exposure.

Broadband instant measurements are often insufficient, since the evaluated transmitters do not always operate at maximum power, for example, in the case of base stations, the transmitted power is dependent on the traffic. In such cases, information on the maximum exposure with respect to the measured exposure must be available and soundly applied to extrapolate the worst-case exposure. Table 11.3 lists the parameters that are necessary to extrapolate the worst-case exposure and to reduce the uncertainty of the actual measurement campaign. It is easier to determine the measurement methods when additional parameters are known. General sources of error are:

- Field perturbation by measurement personnel, for instance, reflection and absorption of EMF due to the body of the measurement engineer
- Application of the measurement antenna, for example, nonobservance of antenna directivity and polarization
- Application of ineffectively decoupled cables, for instance, acting as secondary antennas

TABLE 11.3

Important Parameters of RF Transmitter Sites Assessed in the Far Field

Site Parameter	Explanation
Location	The location of the transmitter with respect to the measurement point
Line of sight/nonline of sight	Determines if a prevalent propagation path may be expected
Type of site	Single- or multiple-antenna site
Antenna directivity	Antenna beam characteristics
Antenna radiation direction	The direction the transmitter radiates
Antenna power at measurement	The antenna input power at the time the measurement takes place
Maximum antenna input power	Maximum permissible antenna input power
Frequency	Frequencies at which the site transmits
Communication system	Communication system that is used, that is, which signal characteristics are expected
Other sources of radiation	The field at the measurement point if the assessed transmitter is switched off

- Application of the measurement receiver, for example, incorrect measurement settings
- Selection of the measurement point, for example, measurement points that are not feasible to give the maximum EMF exposure, measurement points close to bodies that influence the measurement antenna's calibration.

Different methods for assessing EMF exposure in the far field have been proposed. One approach is the scanning method. This method requires the engineer to slowly move the measurement antenna with varying polarizations and directions through the volume of interest [53]. The measurement receiver operates in maximum hold mode during the assessment, that is, the maximum field value is determined and compared to the reference values. Another method is based on the examination of several well-defined points in the area of interest. In this case, the antenna is mounted on a tripod, and the different directions and polarizations are examined at the considered points [54]. The first method is conservative but sensitive to the position of the measurement operator with respect to the antenna. The second method can be performed with the measurement engineer further away, but the number of measurements in the volume is small. A combination of both methods is presented in Coray et al. [55], that is, first the region is scanned for the field maximum in the area of interest, and then an isotropic and frequency-selective measurement is performed at the location of the maximum.

Far-field techniques are also often employed in the near field of transmitters, for example, on transmitter towers. Some standards allow a spatial averaging of E field evaluations [9], the rationale of which is based on the whole-body SAR limit. However, this constitutes a relaxation of the safety concept, since it does not consider H field coupling as the dominant mechanism in the near field nor the limits of peak spatial SAR. Based on current knowledge, such relaxations do not exclude violations of the basic restrictions.

The advantages and limitations of different measurement techniques to assess exposure from unknown transmitters are discussed below.

11.5.1 Broadband Measurements

Broadband measurements are especially applicable for survey measurements. The field is measured and automatically summed over a broad frequency range. No information on

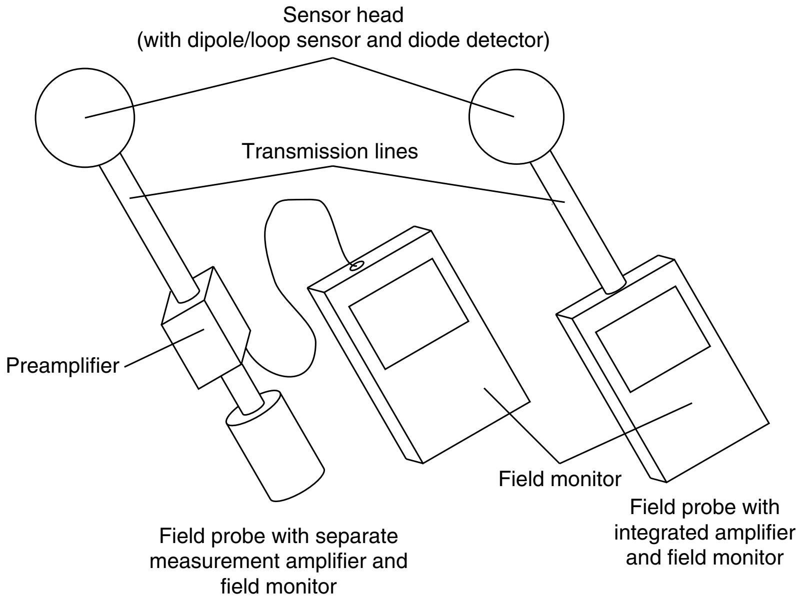

FIGURE 11.12
Schematic of the most common designs of broadband RF survey meters.

the spectral characteristics of the field is available. Therefore, if a broadband meter is used for compliance testing, the measured field value must comply with the lowest permissible limit defined in the measurement range of the meter. Broadband survey meters are relatively inexpensive and easy to apply. Hence, these probes are often used for field measurements.

Figure 11.12 displays typical broadband field survey meter designs. Figure 11.13 displays the frequency response of two broadband probes. The field value measured with probe 1 must comply with the lowest limit in the frequency range from 10 MHz to 1 GHz, whereas probe 2 must comply with the lowest limit between 100 MHz and 10 GHz. The overlapping frequency range is counted twice if the exposure values are added to cover the entire frequency range. Some broadband probes are designed to reflect the frequency dependence of the limits. In all cases, it is advised that the off-band response of

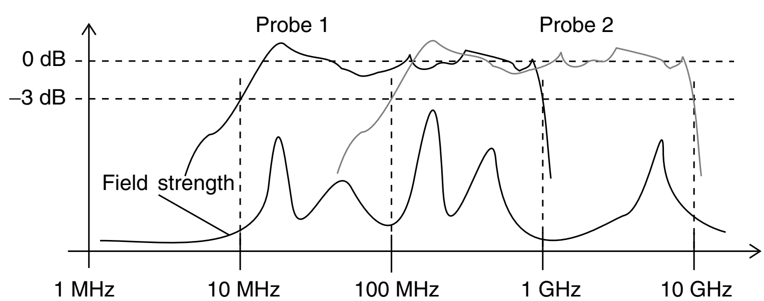

FIGURE 11.13
Frequency response of two broadband field survey meters. The fields in the frequency ranges are summed up. If the fields from probes 1 and 2 are summed again, then the fields in the overlapping frequency range are accounted for twice.

these probe systems be carefully evaluated. If a specific transmitter is the dominant source, compliance testing is greatly simplified [56].

In addition to the frequency response, broadband probes have a certain time-domain transfer function. When pulsed fields are measured, this response must be compensated. However, for this compensation, information on the time-domain characteristics of the measured field is necessary. In summary, the main sources of uncertainty regarding broadband survey meters are:

- Calibration
- Linearity
- Frequency response
- Isotropy
- Time-domain response
- Temperature response

In conclusion, the accuracy of broadband evaluations is significantly limited but generally conservative.

11.5.2 Frequency-Selective Measurements

Frequency-selective measurement techniques can overcome the issue of the unknown spectral composition of the field. However, the execution of the measurement is more complicated, such that insufficiently trained personnel are likely to produce erroneous results.

Measurements in the frequency domain are performed with a measurement antenna, as described in Section 11.3.3, that is connected to a spectrum analyzer (Figure 11.14). The spectrum analyzer mixes the received RF signal down to the base band. A filter is swept in frequency over the considered sweep bandwidth. The signal after the filter is detected using user-definable detectors. Most spectrum analyzers provide video filters for additional filtering (smoothing) of the spectral signal. Setting the sweep and filter parameters can significantly impact the measurement result. Optimal settings for GSM and Universal Mobile Telecommunications System (UMTS) based on a simulation approach were recently presented by Olivier and Martens [57]. The impact of summing up parts of the spectrum because of nonideal filters was investigated by Joseph et al. [58]. Modern analyzers also provide a zero-span mode. The RF signal is mixed down to the base band, and only the time-domain envelope of the signal is displayed afterward. This mode may be applied, for example, to investigate the time-domain characteristics of an unknown communication system. Additionally, it is especially useful to measure pulsed

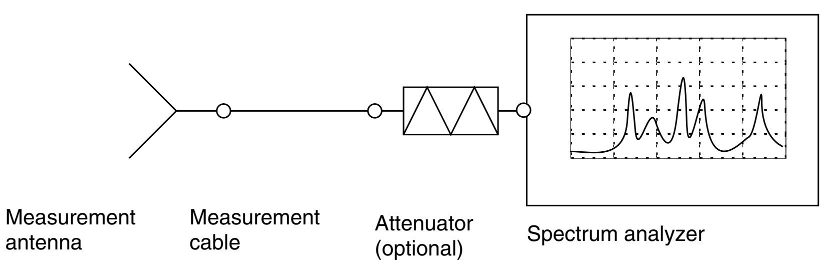

FIGURE 11.14
Schematic of a frequency-selective measurement of EMF.

signal forms, as this signal form is often used in communication systems. In summary, the application of spectrum analyzers is a complex subject. Measurement recommendations dealing with frequency-selective measurements should always describe the spectrum analyzer settings to produce feasible and comparable results. Nevertheless, the measurement engineer should still test the actual applicability of these settings for his particular measurement equipment.

The main sources of uncertainty regarding frequency-selective measurements are:

- Calibration of the spectrum analyzer, cable, and measurement antenna
- Linearity of the spectrum analyzer, cable, and measurement antenna
- Frequency response of the spectrum analyzer, cable, and measurement antenna
- Demodulation method of the spectrum analyzer (detector type)
- Temperature response of the spectrum analyzer, cable, and measurement antenna
- Mismatch between measurement equipment

Although the frequency-selective measurement method overcomes most of the issues regarding broadband survey meters, it is not sufficient to soundly identify the exposure from different transmitters at the same frequency. In this case, measurement receivers should be applied.

11.5.3 Code-Selective Measurements

Code-selective measurements are especially necessary if the exposure from a specific transmitter applies code division multiple access (CDMA), for example, if a UMTS is to be assessed. In the case of UMTS, all base stations usually transmit in a single-frequency band. With a frequency-selective receiver, it is not possible to discriminate between exposure from different base stations, since a single-frequency band is used and the channels are multiplexed in the code domain. Code-selective receivers decode the signal received from a base station, that is, the receiver is able to discriminate between a field strength received from the base station of interest and other noise-like sources. The receiver measures the field received from the base station of interest only if the particular scrambling code is used for decoding. Basically, the same sources of uncertainty must be considered for code- and frequency-selective measurements. However, in contrast to frequency-selective measurements, the modulation of the signal does not increase the uncertainty but rather the possible nonorthogonality of the respective scrambling codes. Many of the typical measurement receivers for UMTS base station measurements (e.g., Rohde and Schwarz TSMU [59], Anritsu ML8720B [60]) provide insufficient sampling rates for swept scanning. Others overcome this limitation, for example, Narda-STS SRM-3000 [61].

11.6 Typical Maximum Peak Spatial SAR Exposures

The daily local RF exposure of the general public has increased by several orders of magnitude with the introduction and proliferation of mobile handsets. This has triggered concern among health agencies and the public, since the highest exposed tissue is the brain. Figure 11.15 and Figure 11.16 display the frequency of worst-case SAR from mobile phones measured according to Refs. [62,63]. Figure 11.15 represents the typical SAR

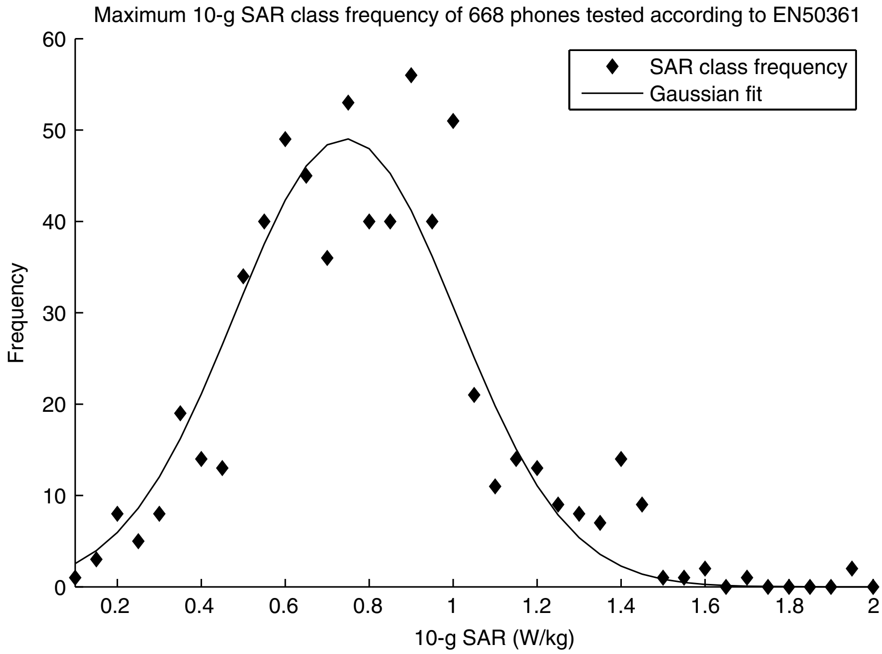

FIGURE 11.15
Statistical distribution of maximum 10-g SAR measured for 668 mobile phones according to EN50361. (From German Federal Office for Radiation Protection, http://www.bfs.de/elektro/hff/oekolabel.html, 2005.)

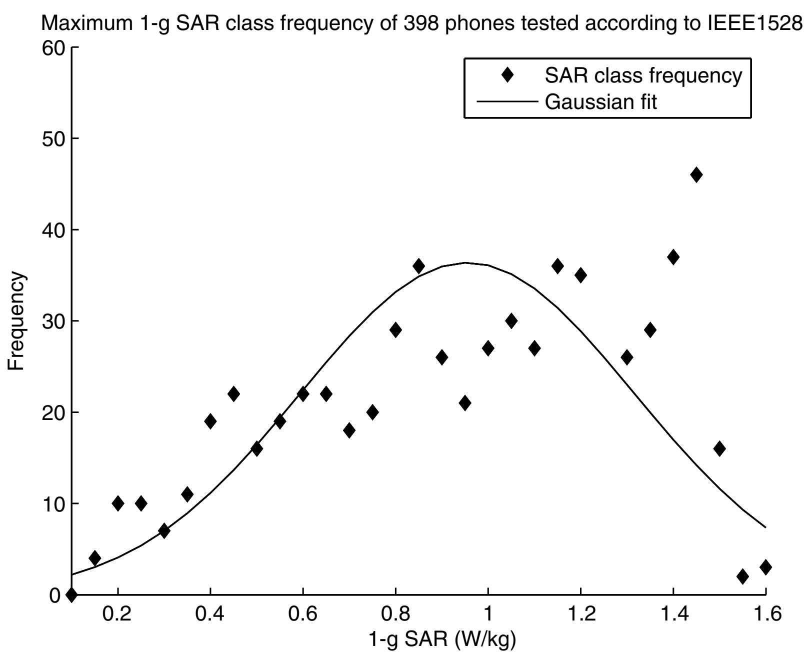

FIGURE 11.16
Statistical distribution of maximum 1-g SAR measured for 687 mobile phones according to IEEE-1528. (From Federal Communications Commission, http://www.fcc.gov/cgb/sar/, 2005.)

TABLE 11.4

Worst-Case Peak Spatial SAR of a Set of Wireless Indoor Devices

Device Class	Frequency Range (MHz)	Worst-Case 10-g SAR (W/kg)
Baby surveillance	40–863	0.077
DECT	1880–1900	0.055
WLAN	2400–2484	0.81
Bluetooth	2402–2480	0.49
PC peripherals	27–40	≤0.005

Note: An absolute worst case for all commercially available products cannot be estimated based on these data.

values for Europe (mean 10-g SAR: 0.74) [64] and Figure 11.16 for North America (mean 1-g SAR: 0.96) [65]. The different averaging masses are due to different legal regulations in Europe and the United States. These values are a considerable percentage of the limits. A recent statistical analysis of the Federal Communications Commission (FCC) SAR database found that the SAR values of newer phones are typically lower than of older phones despite their greatly reduced size.

SAR measurements of devices operated in home and office environments were reported by Kramer et al. [66]. A summary of the maximum SAR values determined in this study for several types of transmitters is given in Table 11.4. It should be noted that under worst-case scenarios, the SAR values measured for WLAN and Bluetooth communication systems are in the same range as those for mobile phones.

11.7 Typical Far-Field Exposures

A study regarding indoor incident field exposure from cellular base station sites was conducted by ARCS (Austria) [55] in the city of Salzburg. Table 11.5 shows two

TABLE 11.5

Results from Indoor Incident *E* Field Measurements Conducted in an Austrian City [55]

Base Station	Distance to Base Station (m)	Cumulative Incident *E* Field (V/m)	Distance to Base Station (m)	Cumulative Incident *E* Field (V/m)
1	196	0.37	374	0.35
2	88	0.51	108	0.89
3	9	0.034	15	0.037
4	16	0.62	8	1.00
5	85	0.94	152	0.75
6	81	1.8	85	1.71
7	4	3.7	25	1.02
8	93	0.19	208	0.19
9	34	0.40	55	0.63
10	39	1.9	76	2.8
11	174	0.59	220	0.45
12	41	0.70	107	0.67
13	2.5	0.67	5.5	0.15

Note: Two cumulative incident field exposure values (sum of incident field exposures from multiple transmitters at one site) at different distances are shown as exemplary for each base station site.

TABLE 11.6

Worst-Case *E* Field of Typical Wireless Indoor Devices at 20-cm and 1-m Distance

Device Class	Frequency Range (MHz)	Worst-Case *E* Field (V/m) (20 cm)	Worst-Case *E* Field (V/m) (1 m)
Baby surveillance	40–863	8.5	3.2
DECT	1880–1900	11.5	2.9
WLAN	2400–2484	3.9	1.1
Bluetooth	2402–2480	3.1	1.0
PC peripherals	27–40	$\leq$1.5	$\leq$1.5

cumulative incident field exposure values (sum of incident field exposures from multiple transmitters at one site) measured at different distances from the considered base station sites. The values are within 0.1 to 1 V/m for distances up to several hundreds of meters. These data also underline that the distance to the base station site has a poor correlation for the incident exposure.

Similar results were reported by Bornkessel and Schubert [67]. This study also included outdoor measurement points and addressed the time dependence, that is, traffic dependence of the exposure from cellular base stations. The results showed a significant time dependence for base stations with multiple traffic channels. In these cases, clearly lower exposure can be expected at night and on weekends.

The incident field exposures from typical devices used in home and office environments were assessed by Kramer et al. [66]. The maximum *E* field exposure values for different device categories are summarized in Table 11.6. The incident field exposure from cellular base stations may be exceeded by the exposure from these devices because of the generally closer distances.

Additionally, an incident exposure of 1 V/m translates to a peak spatial SAR value in the brain that is approximately a factor 10,000 times lower than the maximum exposure by a handset. Thus, exposure by handsets is by far the most dominant source of RF exposure for the general population.

Acknowledgment

The authors wish to thank Prof. Dr. Quirino Balzano, Dr. Urs Lott, and Dr. Katja Pokovic for their critical review of this manuscript. The dosimetric research at the IT'IS Foundation is supported by many institutions, the most significant of which are European and Swiss Funding Agencies, Motorola Inc. (USA), the Mobile Manufacturers Forum (Belgium), MTT (Japan), and Schmid & Partner Engineering AG (SPEAG, Switzerland).

References

1. Schmid, G., Neubauer, G., Illievich, U.M., and Alesch, F., ''Dielectric properties of porcine brain tissue in the transition from life to death at frequencies from 800 to 1900 MHz,'' *Bioelectromagnetics*, Vol. 24, No. 6, Sept. 2003, pp. 413–422.

2. Poković, K., Advanced Electromagnetic Probes for Near-Field Evaluations, Ph.D. thesis, Diss. ETH Nr. 13334, Zurich, Switzerland, 1999.
3. Schönborn, F., Poković, K., and Kuster, N., ''Dosimetric analysis of the carousel setup for the exposure of rats at 1.62 GHz,'' *Bioelectromagnetics*, Vol. 25, No. 1, Jan. 2004, pp. 16–26.
4. Christ, A., Chavannes, N., Nikoloski, N., Gerber, H.-U., Poković, K., and Kuster, N., ''A numerical and experimental comparison of human head phantoms for compliance testing of mobile telephone equipment,'' *Bioelectromagnetics*, Vol. 26, No. 2, Feb. 2005, pp. 125–137.
5. Kainz, W., Christ, A., Kellom, T., Seidman, S., Nikoloski, N., Beard, B., and Kuster, N., ''The specific anthropomorphinc mannequin (SAM) compared to 14 anatomical head models using a novel definition for the mobile phone positioning,'' *Physics in Medicine and Biology*, Vol. 50, No. 14, July. 2005, pp. 3423–3445.
6. Kuster, N., Schuderer, J., Christ, A., Futter, P., and Ebert, S., ''Guidance for exposure design of human studies addressing health risk evaluations of mobile phones,'' *Bioelectromagnetics*, Vol. 25, No. 7, Oct. 2004, pp. 524–529.
7. ICNIRP, ''Guidelines for limiting exposure to time-varying electric, magnetic, and electromagnetic fields (up to 300 GHz),'' *Health Physics*, Vol. 74, No. 4, 1998, pp. 494–522.
8. ANSI/IEEE, *C95.6–2002, IEEE Standard for Safety Levels with Respect to Human Exposure to Electromagnetic fields, 0–3 kHz*, The Institute of Electrical and Electronics Engineers, Inc., New York, 2002.
9. ANSI/IEEE, *C95.1–2001, IEEE Standard for Safety Levels with Respect to Human Exposure to Radio Frequency Electromagnetic Fields, 3 kHz to 300 GHz*, The Institute of Electrical and Electronics Engineers, Inc., New York, 2001.
10. National Council on Radiation Protection and Measurements (NCRP), Ed., *Biological Effects and Exposure Criteria for Radiofrequency Electromagnetic Fields*, NCRP, 1986.
11. Aslan, E., ''Electromagnetic radiation survey meter,'' *IEEE Transactions on Instrumentation and Measurement*, Vol. IM-19, No. 4, 1970, pp. 368–372.
12. Rudge, A.W., ''An electromagnetic radiation probe for near-field measurements at microwave frequencies,'' *Journal of Microwave Power*, Vol. 5, No. 3, 1970, pp. 155–174.
13. Bassen, H., Swicord, M., and Abita, J., ''A miniature broad-band electric field probe,'' *Annals of the New York Academy of Sciences, Biological Effects of Nonionizing Radiation*, Vol. 247, No. 2, Feb. 1975, pp. 481–493.
14. Bassen, H., Herman, W., and Hoss, R., ''EM probe with fiber optic telemetry system,'' *Microwave Journal*, Vol. 20, No. 4, Apr. 1977, pp. 35–47.
15. Bassen, H.I. and Smith, G.S., ''Electric field probes—a review,'' *IEEE Transactions on Antennas and Propagation*, Vol. 31, No. 5, 1983, pp. 710–718.
16. Hopfer, S., ''The design of broad-band resistive radiation probes,'' *IEEE Transactions on Instrumentation and Measurements*, Vol. IM–21, No. 4, Nov. 1972, pp. 416–421.
17. Smith, G., ''Analysis of miniature electric field probes with resistive transmission lines,'' *IEEE Transactions on Microwave Theory and Techniques*, Vol. MTT–29, No. 11, Nov. 1981, pp. 1213–1224.
18. Schmid, T., Egger, O., and Kuster, N., ''Automated E-field scanning system for dosimetric assessments,'' *IEEE Transactions on Microwave Theory and Techniques*, Vol. 44, No. 1, Jan. 1996, pp. 105–113.
19. Whiteside, H. and King, R., ''The loop antenna as a probe,'' *IEEE Transactions on Antennas and Propagation*, Vol. AP–12, No. 5, May 1964, pp. 291–297.
20. Kanda, M., ''Standard probes for electromagnetic field measurement,'' *IEEE Transactions on Antennas and Propagation*, Vol. AP–41, No. 10, Oct. 1993, pp. 1349–1364.
21. Narda Safety Test Solutions, ''Electric field probe for EMR-200 and EMR-300,'' http://www.narda-sts.com, 2005, accessed Dec. 16, 2005.
22. SPEAG Switzerland, ''SPEAG dosimetric near-field probes (product flyer),'' http://www.dasy4.com/flyers/probes.pdf, 2005, accessed Dec. 16, 2005.
23. Poković, K., Schmid, T., and Kuster, N., ''Millimeter-resolution E-field probe for isotropic measurement in lossy media between 100 MHz and 20 GHz,'' *IEEE Transactions on Instrumentation and Measurements*, Vol. 49, No. 4, Aug. 2000, pp. 873–878.

24. Poković, K., Schmid, T., Fröhlich, J., and Kuster, N., ''Novel probes and evaluation procedures to assess field magnitude and polarization,'' *IEEE Transactions on Electromagnetic Compatibility*, Vol. 42, No. 2, May 2000, pp. 240–245.
25. Cecelja, F. and Balachandran, W., ''Optimized CdTe sensors for measurement of electric and magnetic fields in the near-field region,'' *IEEE Transactions on Instrumentation and Measurements*, Vol. 49, No. 3, June 2000, pp. 483–487.
26. Tokano, Y., Kobayashi, H., and Miyakawa, T., Houjyo, Y. ''A gigahertz-range micro optical electric field sensor,'' in *Electromagnetic Compatibility 2001*, Zurich, Switzerland, 2001, p. 127.
27. Tajima, K., Kobayashi, R., Kuwabara, N., and Tokuda, M., ''Development of optical isotropic E-field sensor operating more than 10 GHz using Mach–Zehnder interferometers,'' *IEICE Transactions on Electronics*, Vol. 85, 2002, p. 961.
28. Agullo-Lopez, F., Cabrera, J., and Agullo-Rueda, F., *Electrooptics*, Academic Press, New York, 1994.
29. Rigrod, W.W. and Kaminow, I.P., ''Wide-band microwave light modulation,'' *IEEE*, Vol. 51, Jan. 1963, pp. 137–140.
30. Lei, C. and Kilcoyne, S., Eds., ''Vertical-cavity surface-emitting lasers VI,'' in *Proceedings of SPIE*, SPIE—The international society for optical engineering, 2002.
31. Choquette, K. and Lei, C., Eds., ''Vertical-cavity surface-emitting lasers V,'' in *Proceedings of SPIE*, SPIE—The international society for optical engineering, 2001.
32. Wilmsen, C., Temkin, H., and Coldren, L., *Vertical-Cavity Surface-Emitting Lasers*, Cambridge University Press, The Edinburgh Building, Cambridge CB2 2RU, U.K. 1999.
33. Schuderer, J., EMF Risk Assessment: In Vitro Research and Sleep Studies, Ph.D. thesis, Diss. ETH Nr. 15347, Zurich, Switzerland, 2003.
34. Bowman, R.-R., ''A probe for measuring temperature in radio-frequency heated material,'' *IEEE Transactions on Microwave Theory and Techniques*, Vol. 24, 1976, pp. 43–45.
35. Burkhardt, M., Poković, K., Gnos, M., Schmid, T., and Kuster, N., ''Numerical and experimental dosimetry of petri dish exposure setups,'' *Journal of the Bioelectromagnetic Society*, Vol. 17, No. 6, 1996, pp. 483–493.
36. Schuderer, J., Schmid, T., Urban, G., Samaras, T., and Kuster, N., ''Novel high resolution temperature probe for RF dosimetry,'' *Physics in Medicine and Biology*, Vol. 49, No. 6, Mar. 2004, pp. N83–N92.
37. Wickersheim, K.-A. and Sun, M.-H., ''Fiberoptic thermometry and its application,'' *Journal of Microwave Power*, Vol. 22, 1987, pp. 85–93.
38. Guy, A.W., ''Analyses of electromaagnetic fields induced in biological tissue by thermographic studies on equivalent phantom models,'' *IEEE Transactions on Microwave Theory and Techniques*, Vol. 34, No. 6, June 1971, pp. 671–680.
39. Taurisano, M.D. and Vorst, A.V., ''Experimental thermographic analysis of thermal effects induced on a human head exposed to 900 MHz fields of mobile phones,'' *IEEE Transactions on Microwave Theory and Techniques*, Vol. 48, No. 11, Nov. 2000, pp. 2022–2032.
40. Baba, M., Suzuki, Y., Taki, M., Fukunaga, K., and Watanabe, S., ''Three dimensional visualization of the temperature distribution in a phantom for the assessment of localized exposure to microwaves,'' in *Biolelectromagnetic Society 2005 Annual Meeting*, Bioelectromagnetic Society, Dublin, Ireland, June 2005, pp. 250–251.
41. Durney, C.H., Massoudi, H., and Iskander, M.F., *Radiofrequency Radiation Dosimetry Handbook*, 4th ed. Brooks Air Force, Brooks Air Force Base, TX, 1997.
42. Seibersdorf Research, Austria, ''Precision conical dipole PCD 8250,'' http://www.seibersdorf-rf.com/docs/leaflet/W_ Products_PCD8250_engl_.pdf, 2005, accessed Dec. 16, 2005.
43. Seibersdorf Research, Austria, ''Precision biconical antenna PBA 320,'' http://www.seibersdorf-rf. com/docs/leaflet/W_ Products_PBA320_engl.pdf, 2005, accessed Dec. 16, 2005.
44. Müller, W. and Georg Neubauer, H.H., ''ADD3D, a new technique for precise power flux density measurements at mobile communications base stations,'' http://www.seibersdorf-rf.com/docs/pubdl/Pub4_Add3Denglish.pdf, 2000, accessed Dec. 16, 2005.

45. Drossos, A., Santomaa, V., and Kuster, N., ''The dependence of electromagnetic energy absorption upon human head tissue composition in the frequency range of 300–3000 MHz,'' *IEEE Transactions on Microwave Theory and Techniques*, Vol. 48, No. 11, Nov. 2000, pp. 1988–1995.
46. Kanda, M.Y., Douglas, M.G., Mendivil, E.D., Ballen, M., Gessner, A.V., and Chou, C.-K., ''Faster determination of mass-averaged SAR from 2-D area scans,'' *IEEE Transactions on Microwave Theory and Techniques*, Vol. 52, No. 8, 2004, pp. 2013–2020.
47. Merckel, O. and Fleury, G., ''Rapid SAR measurement of mobile phones,'' *International Symposium on International Journal of Applied Electromagnetics and Mechanics*, Vol. 19, 2004, pp. 183–186.
48. TEM Consulting, ''Near field RF scanner,'' http://www.temconsulting. com/Products/Scanning Positioner/RF_Scanner.htm, 2005, accessed Dec. 16, 2005.
49. Chavannes, N., Tay, R., Nikoloski, N., and Kuster, N., ''Suitability of FDTD based TCAD tools for RF design of mobile phones,'' *IEEE Antennas and Propagation Magazine*, Vol. 45, Dec. 2003, pp. 52–66.
50. ANSI C63.19, ''American National Standard for Methods of Measurement of Compatibility between Wireless Communications Devices and Hearing Aids (Revision Draft 3.8),'' Oct. 2005.
51. Ogawa, K., Ozaki, A., Kajiwara, S., Yamamoto, A., Koyanagi, Y., and Saito, Y., ''High-speed SAR prediction for mass production stages in a factory by H-field measurements,'' *IEEE Antennas and Propagation Society Symposium, 2004*, Vol. 2, June 2004, pp. 1843–1846.
52. Kuster, N. and Balzano, Q., ''Experimental and numerical dosimetry,'' in *Mobile Communications Safety*, Kuster, N., Balzano, Q., and Lin, J.C., Eds. Chapman & Hall, London, 1996, pp. 13–64.
53. Abteilung Nichtionisierende Strahlung, Mobilfunk Basisstationen (GSM) Messempfchlung, Technical report, BUWAL, Switzerland, 2002.
54. ANFR, Protocol de measure *in situ*, Technical Report 2.1, Agence National des Frequences, France, May 2004.
55. Coray, R., Krähenbühl, P., Riederer, M., Stoll, D., Neubauer, G., and Szentkuti, B., Immissionen in Salzburg, Technical Report, BAKOM, Switzerland, 2002.
56. CENELEC EN 50400, ''Basic standard to demonstrate the compliance of fixed equipment for radio transmission (110 MHz–40 GHz) intended for use in wireless telecommunication networks with the basic restrictions or the reference levels related to general public exposure to radio frequency electromagnetic fields, when put into service,'' Sept. 2005.
57. Olivier, C. and Martens, L., ''Optimal settings for frequency selective electromagnetic field measurements for exposure assessment around base stations,'' In *Biolelctromagnetic Society 2005 Annual Meeting*, Bioelectromagnetic Society, Dublin, Ireland, June 2005, pp. 466–468.
58. Joseph, W., Olivier, C., and Martens, L., ''A robust, fast and accurate deconvolution algorithm for EM-field measurements around GSM and UMTS base stations with a spectrumanalyser,'' *IEEE Transactions on Instrumentation and Measurements*, Vol. 51, No. 6, Feb. 2003, pp. 1163–1169.
59. Rohde and Schwarz, Germany, ''Radio network analyzer R&S TSMU,'' http://www.rohde-schwarz.com/www/download_files.nsf/file/TSMU_en.pdf/-$file/TSMU_en.pdf, 2004, accessed Dec. 16, 2005.
60. Anritsu, Japan, ''ML8720B UMTS/W-CDMA field strength area tester,'' http://www.eu.anrit-www.eu.anritsu.com/files/ML8720B_E11000.pdf, 2005, accessed Dec. 16, 2005.
61. Narda Safety Test Solutions, ''SRM-3000 frequency-selective field strength measuring system for rapid, reliable safety assessments,'' http://www.narda-sts.com, 2005, accessed Dec. 16, 2005.
62. CENELEC EN 50361, ''Basic standard for the measurement of specific absorption rate related to human exposure to electromagnetic fields from mobile phones (300 MHz–3 GHz),'' 2001.
63. IEEE SC34, Recommended Practice for Measurements and Computations with Respect to Human Exposure to Radio Frequency Electromagnetic Fields, 100kHz to 300 GHz (IEEE Standard C95.3), Technical report, IEEE, 2002.
64. German Federal Office for Radiation Protection, ''Strahlenschutzkriterien für ein Mobiltelefon-Ökolabel,'' http://www.bfs.de/elektro/hff/oekolabel.html, 2005, accessed Dec. 16, 2005.
65. Federal Communications Commission, ''FCC SAR database,'' http://www.fcc.gov/cgb/sar/, 2005, accessed Dec. 16, 2005.
66. Kramer, A., Kühn, S., Lott, U., and Kuster, N., Development of Procedures for the Assessment of Human Exposure to EMF from Wireless Devices in Home and Office Environments, Technical

report, IT'IS Foundation for Research on Information Technologies in Society, Zurich, Switzerland, Jan. 2005.
67. Bornkessel, C. and Schubert, M., Zwischenbericht: Analyse der Immissionsverteilung, Technical report, IMST GmbH Kamp-Lintfort, 2004.
68. van Deventer, E., Simunic, D., and Repacholi, M., EMF Standards for human health, in *Biological and Medical Aspects*, Barnes, F.S. and Greenebaum, B., Eds., Taylor & Francis, Boca Raton, FL, 2006, Chapter 8.